IVS Memorandum 2012-001v01

4 May 2012

"Observations of ICRF2 Sources to Improve the Astrometry of the Future Radio-optical Transfer Sources"

Geraldine Bourda, Patrick Charlot

VLBI observing proposal to the IVS

Preparing the VLBI celestial reference frame for the Gaia era: Observations of ICRF2 sources to improve the astrometry of the future radio–optical transfer sources

G. Bourda & P. Charlot
Laboratoire d'Astrophysique de Bordeaux
Univ. Bordeaux, CNRS, F-33270, Floirac, France

4 May 2012

Abstract

The European space astrometry mission Gaia will construct a dense optical QSO-based celestial reference frame. For consistency between optical and radio positions, it will be fundamental to align the Gaia and VLBI frames with the highest accuracy. A proper alignment is also important for astrophysics, for example to probe the AGN jets properties and the physics of these objects. The VLBI-Gaia frame alignment requires quasars that are bright at optical wavelength, that have a compact radio core, and that do not exhibit complex structures. In this proposal, we give the list of suitable ICRF2 sources to observe further in order to optimize the VLBI-Gaia frame alignment. This sample is composed of 195 radio sources. We recommend that these sources be monitored to check their relevance for the alignment, especially in terms of position stability and structures. We also draw plans for future observations during the Gaia mission.

1   Context

The ESA space astrometry mission Gaia, to be launched in June 2013, will survey all stars and QSOs (Quasi Stellar Objects) down to an apparent optical magnitude of 20 (Perryman et al., 2001). Optical positions with Gaia will be determined with an unprecedented accuracy, ranging from 10–70 microarcseconds (μas) at magnitude 14–18 to 200 μas at magnitude 20 (Lindegren et al., 2008). Based on current estimates from local surveys, it is anticipated that 500 000 such QSOs should be detected. Of these, only the objects with the most accurate positions (i.e. brighter than magnitude 18) will be used to define the frame. Simulations show that the residual spin of the Gaia frame could be determined to 0.5 μas/yr with a "clean sample" of 10 000 sources (Mignard, 2002). A preliminary Gaia catalog is expected to be available by 2015 with the final version released by 2020.

During the past decade, the IAU (International Astronomical Union) fundamental celestial reference frame was the ICRF (International Celestial Reference Frame; Ma et al. 1998; Fey et al. 2004), composed of the VLBI positions of 717 extragalactic radio sources. Since 1 January 2010, this first realization has been superseded by the new and more accurate ICRF2 (IERS Technical Note 35, 2009). The ICRF2 includes VLBI coordinates for 3 414 extragalactic radio sources, with a floor in position accuracy of 60 μas and an axis stability of 10 μas.

The alignment between the future Gaia frame and the ICRF2, or its successor by 2020, will be crucial not only for guaranteeing a proper transition if the fundamental celestial reference frame is moved from the radio to the optical domain, but also to register the radio

1

and optical images of any celestial target with the highest accuracy, which would be of high astrophysical interest. For example, it will allow one to pinpoint the relative location of the optical and radio emission for hundreds of active galactic nuclei (AGN) to a few tens of μas, placing constraints on the overall AGN geometry.

Aligning the optical and radio reference frames requires several hundreds of common objects, with a sky coverage as uniform as possible in order to detect and correct any potential local deformations of the frames. The more objects, the more accurate the link, since the accuracy in the orientation of the frame axes scales as $\sqrt{n}$, where n is the number of objects. This alignment, to be determined with the highest accuracy, also requires the common sources to have very accurate radio and optical positions. Obtaining such accurate positions implies that the link sources must be brighter than magnitude 18 (as mentioned above) without any extended VLBI structures (for the highest VLBI astrometric accuracy).

Applying these criteria, we found in a previous study that only 10% of the sources from the ICRF (70 sources) were suitable for this purpose (Bourda et al., 2008). With the advent of the ICRF2, which is based on 4–5 times more sources, the number of suitable sources increased and about 200 were found to meet the criteria (Bourda and Charlot, 2012). In this proposal, we focus on such transfer sources and request that their observations within the IVS are intensified. The procedure to obtain this list of sources is explained in Sect. 2 below, as well as the suggested observing plan to strengthen the astrometry of these sources (Sect 3.1). We also describe supplementary observations that are carried out with other VLBI networks to optimize this alignment (Sect. 3.2).

2 This proposal: Source selection

In order to identify the ICRF2 sources suitable for the alignment with the future Gaia frame, we cross-identified this radio catalogue with the LQAC2 (Large Quasar Astrometric Catalogue 2; Souchay et al. 2012), a compilation of several quasar catalogues with optical information on magnitudes (187 504 objects). By cross-correlating these two catalogues (with a cut-off value of 3″; see Table 1 for the results), one can highlight that:

- 72% of the ICRF2 sources will be observable with Gaia (i.e. 2 453 sources with $0 < V \leq 20$ or $0 < R \leq 20$ or $0 < I \leq 20$), half of which (1 264 sources) have a proper optical counterpart for the Gaia-alignment (i.e. with $0 < V \leq 18$ or $0 < R \leq 18$ or $0 < I \leq 18$).

- 28% of the ICRF2 sources have either no reliable optical magnitude V, R and I (i.e. 775 sources) or an optical magnitude weaker than 20 (i.e. 186 sources).

Of the 1 264 ICRF2 suitable sources, the repartition in terms of ICRF2 categories is as follows:

- 174 are ICRF2 *defining* sources,

- 438 sources are neither *defining* sources nor part of the VCS catalogue (VLBA Calibrator Survey; Petrov et al. 2008 and references therein),

- 652 sources are only part of VCS catalogue.

Table 1: Number of ICRF2 sources cross-identified within LQAC2, depending on the value and the type of the magnitude (cross-identification cut-off value of 3″).

Magnitude	0 < mag ≤ 20	0 < mag ≤ 19	0 < mag ≤ 18
V	1 345	1 110	568
R	2 343	1 666	869
I	2 113	1 966	1 148
V or R or I	2 453	2 121	1 264

In order to estimate the astrometric quality of these 1 264 optically-suitable ICRF2 sources, we calculated the X-band continuous structure index from the VLBI images available (see IERS Technical Note 35 for more details about this index). In all, structure indices were derived for 33% of this sample (i.e. 420 sources). For this determination, we used the data from IERS TN 35 but also additional images produced since the ICRF2 was built (see the Bordeaux VLBI Image Database; http://www.obs.u-bordeaux1.fr/BVID). The rest of the sources are mostly from the VCS catalogue, and will be investigated in a second stage. From this list, we removed the ICRF2 "special handling sources" (see IERS TN 35) and obtained a sample of 386 sources. Figure 1 shows the X-band continuous structure index distribution for these 386 sources. Among these, 197 sources were found to qualify for the link (i.e. with an X-band structure index < 3.0). From this list, we excluded two sources (0951+693 and 1222+131) that are not compact in the optical domain (Taris 2012, priv. com.). Finally, we end up with a list of 195 transfer sources detailed in Table 2:

- 132 are ICRF2 defining sources,
- 63 are non-defining sources .

Figures 2 and 3, respectively, show the X-band flux density distribution for these 195 sources, and their dissemination on the sky. The latter appears quite homogeneous. The X-band flux density plotted in Figure 2 corresponds to the integrated flux density over the VLBI images (as available from the BVID) and represents the mean value of all measurements over the years. The corresponding values are given in Table 2.

In the future, we plan to update this source list as new data become available (e.g. source structure index determinations). We also plan to extend it by including VCS sources which have not been considered so far.

3   Observing program

With the above list of transfer sources in hand our goal is now to strengthen the astrometry of these sources. We thus request the IVS to include these sources in regular schedules. The proposed observations are detailed in Sect. 3.1 below. To be complete, we also present the additional efforts that we engaged in order to extend the list of transfer sources (Sect. 3.2).

3.1   This proposal: IVS request

As noted above, it is required that the transfer sources have highly-accurate positions in order to obtain the most possible accurate link. Additionally, the sources should also be highly stable in positions. Based on these criteria, our proposal is focused along two directions: (i) improve the astrometry of the transfer sources for which the position accuracy is not yet sufficient; (ii) monitor the positional stability for all transfer sources.

In order to evaluate the number of transfer sources which necessitate a better VLBI positional accuracy, the distribution of VLBI position uncertainty in the ICRF2 catalogue has been plotted (see Figure 4 and Table 2 for the corresponding values). One can notice that more than 70% of the transfer sources (i.e. 144 sources) have a high astrometric position accuracy in the ICRF2 catalogue (i.e. $\sigma < 200$ μas), while the others (51 sources) have less accurate positions (identified with bold-type font in Table 2).

To summarize, this proposal has two observing goals:

1. The first one is devoted to strengthen the VLBI position for the 51 transfer sources identified in Table 2 (bold-type font) which does not have a sufficient positional accuracy (i.e. $\sigma > 200$ μas).

2. The second one is intended to observe all 195 transfer sources on a regular basis in order to monitor their positional stability.

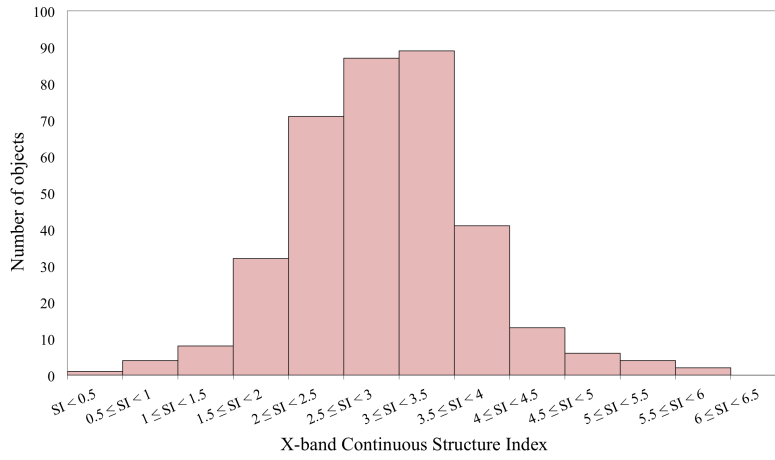Figure 1: Distribution of the X-band continuous structure index, as determined for the 386 optically-bright ICRF2 sources candidate for the Gaia-alignment.
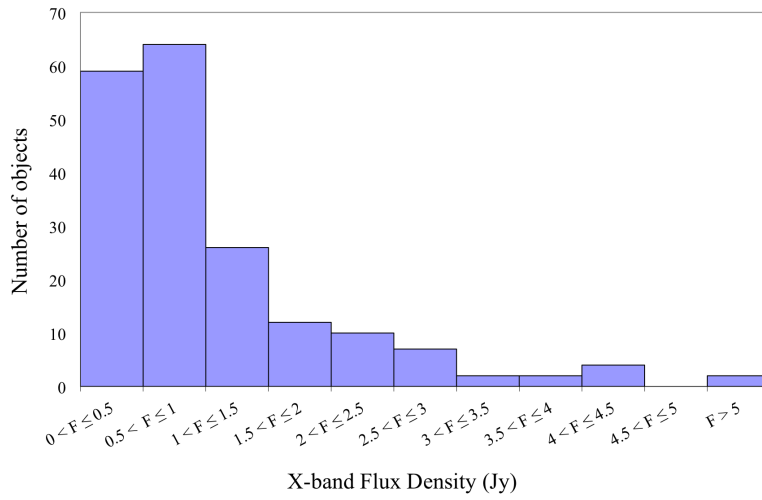

Figure 2: Distribution of the X-band flux density for the 195 ICRF2 transfer sources suitable for the alignment with the Gaia frame (units in Jy).
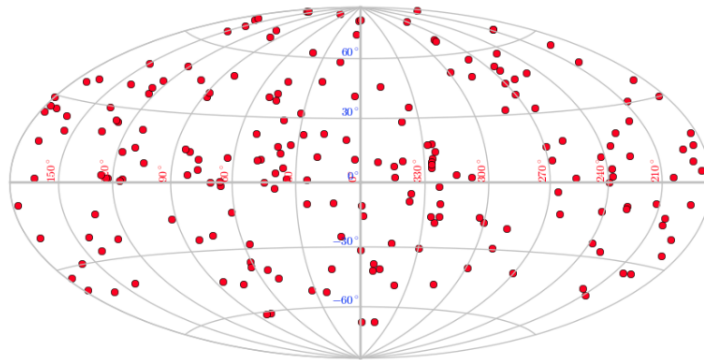

Figure 3: Sky distribution of the 195 ICRF2 transfer sources suitable for the alignment with the Gaia frame.
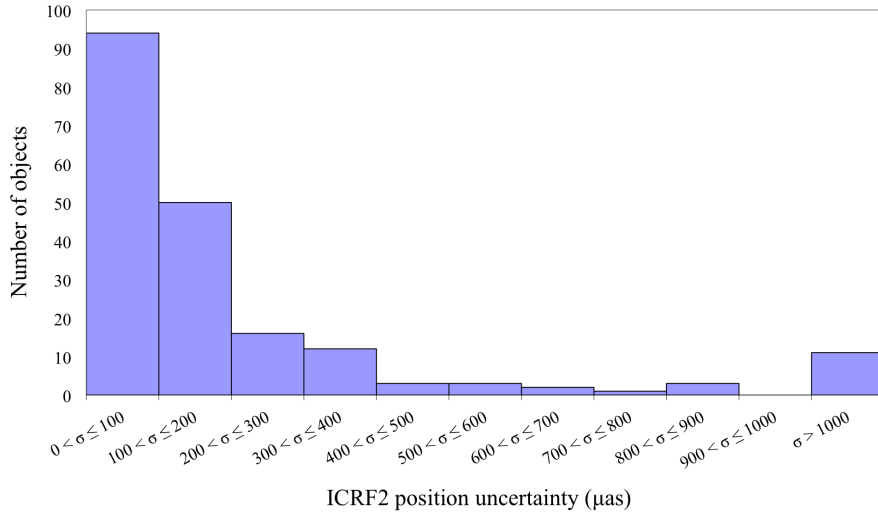
4

Figure 4: Distribution of the ICRF2 position uncertainty for the 195 transfer sources suitable for the alignment with the Gaia frame.

3.2 Supplementary observations

In parallel, efforts have been developed for the last years in order to increase the number of transfer sources for the Gaia-alignment. This is the purpose of a VLBI observing program that we initiated in 2007. This program has been targeted to observe 447 optically-bright extragalactic radio sources, on average 20 times weaker than the ICRF sources, selected from the NRAO VLA Sky Survey (NVSS; Condon et al. 1998), a dense catalogue of weak radio sources. A multi-step VLBI observing strategy has been specifically developed to detect, image, and measure accurate VLBI positions for these sources (Bourda et al., 2010). The first step, whose goal was to assess the VLBI detectability of the targets, showed an excellent detection rate of 89%. In total 398 sources were detected (Bourda et al., 2010). The second step was targeted at imaging the sources previously detected, in order to identify the most point-like sources and therefore the most suitable ones for the alignment. In total, 250 sources could be imaged and about half of them were found to be point-like on VLBI scales (Bourda et al., 2011, 2012). The third step dedicated to VLBI astrometry for the most compact sources will be engaged in 2012 to observe 119 of these sources.

4 Conclusion

The list of ICRF2 transfer sources given in this paper is composed of 195 objects. These sources should be observed regularly by the IVS, in order to strengthen their VLBI position accuracy, as well as to monitor position stability and VLBI structures. This effort is necessary before but also during the Gaia mission. For the latter, it is anticipated that the Gaia scanning law will be used in the future to carry out quasi-simultaneous VLBI and Gaia observations. Such simultaneous observations are desirable to optimize the link between the two frames but is also of strong interest for astrophysical purposes (e.g. to compare locations of optical and radio emission regions).

We do not detail any specific observing schedules for these transfer sources. The choice of the scheduling is left to the appreciation of the IVS Observing Program Committee and schedulers. Updates of this list will be submitted in the future on the basis of new information that may come up (e.g. new VLBI structure indices or optical information).

References

Bourda, G., Charlot, P., & Le Campion, J.-F. 2008, A&A 490, 403

Bourda, G., Charlot, P., Porcas, R., & Garrington, S. 2010, A&A 520, A113

Bourda, G., Collioud, A., Charlot, P., Porcas, R., & Garrington, S. 2011, A&A 526, A102

Bourda, G. 2012, In: DPAC Newsletter 15, ed. F. Mignard, `http://www.rssd.esa.int/index.php?project=GAIA&page=DPAC_Newsletter`

Bourda, G., & Charlot, P. 2012, In: Earth rotation, reference systems and celestial mechanics: Synergies of geodesy and astronomy, Journées 2011 Systèmes de référence spatio-temporels Proceedings, ed. H. Schuh, S. Böhm, T. Nilsson and N. Capitaine, in press

Bourda, G., Collioud, A., Charlot, P., Porcas, R., & Garrington, S. 2012, In: International VLBI Service for Geodesy and Astrometry 2012 General Meeting Proceedings – "Launching the Next-Generation IVS Network", ed. D. Behrend and K. D. Baver, to come

Condon, J. J., Cotton, W. D., Greisen, E. W., et al. 1998, AJ 115, 1693

Fey, A. L., Ma, C., Arias, E. F., et al. 2004, AJ 127, 3587

IERS Technical Note 35 2009, ed. A. L. Fey, D. Gordon and C. S. Jacobs (Frankfurt am Main: Verlag des Bundesamts für Kartographie und Geodäsie), The Second Realization of the International Celestial Reference Frame by Very Long Baseline Interferometry

Lindegren, L., Babusiaux, C., Bailer-Jones, C., et al. 2008, In: "A Giant Step: from Milli- to Micro-arcsecond Astrometry", IAU Symposium No. 248 Proceedings (Cambridge University Press), ed. W. J. Wenjin, I. Platais and M. A. C. Perryman, 217

Ma, C., Arias, E. F., Eubanks, T. M., et al. 1998, AJ 116, 516

Mignard, F. 2002, In: "Gaia: A European Space Project" (EAS Publication series, 2), ed. O. Bienaymé and C. Turon, 327

Ojha, R., Fey, A. L., Johnston, K. J., et al. 2004, AJ 127, 3609

Ojha, R., Fey, A. L., Charlot, P., et al. 2005, AJ 130, 2529

Perryman, M. A. C., de Boer, K. S., Gilmore, G., et al. 2001, A&A 369, 339

Petrov, L., Kovalev, Y., Fomalont, E., & Gordon, D. 2008, AJ 136, 580

Souchay, J., Andrei, A., Barache, C., et al., 2012, "The second release of the Large Quasar Astrometric Catalog (LQAC-2)", A&A 537, A99

Table 2: List of the 195 ICRF2 transfer sources for the alignment with the Gaia frame.

IERS name		α h	m	s	δ °	′	″	$\sigma_{pos.}$ (µas)	X-band flux (Jy)	S-band flux (Jy)
0007+106	D	0	10	31.00590186	10	58	29.5043827	119	0.70	0.25
0010+405	D	0	13	31.13020334	40	51	37.1441040	100	0.45	0.34
0016+731	D	0	19	45.78641940	73	27	30.0174396	154	1.05	0.97
0025+197		0	28	29.81848608	20	0	26.7443060	419	0.15	0.17
0035−252		0	38	14.73550693	−24	59	2.2351862	186	0.73	0.41
0048−097	D	0	50	41.31738756	−9	29	5.2102688	60	0.99	0.75
0059+581	D	1	2	45.76238248	58	24	11.1366009	89	1.65	1.37
0104−408	D	1	6	45.10796851	−40	34	19.9602291	73	2.43	1.13
0109+224	D	1	12	5.82471754	22	44	38.7863909	87	0.46	0.45
0119+115	D	1	21	41.59504339	11	49	50.4131012	60	1.49	1.31
0131−522	D	1	33	5.76255607	−52	0	3.9457209	243	0.54*	
0133+476	D	1	36	58.59480585	47	51	29.1000445	74	2.55	1.85
0137+012		1	39	57.30581788	1	31	46.1384878	869	0.17	0.13
0138−097	D	1	41	25.83215547	−9	28	43.6741894	111	0.74	0.66
0149+218		1	52	18.05904586	22	7	7.6998109	78	0.79	0.80
0202+319	D	2	5	4.92536007	32	12	30.0954538	76	1.64	0.85
0211+171		2	14	44.91285639	17	22	49.5108724	1200	0.10	0.12
0215+015	D	2	17	48.95475182	1	44	49.6990704	85	1.38	0.89
0221+067	D	2	24	28.42819659	6	59	23.3415393	89	0.54	0.42
0229+131	D	2	31	45.89405431	13	22	54.7162668	60	1.20	1.32
0234+285	D	2	37	52.40567732	28	48	8.9900231	63	2.06	1.89
0237−027	D	2	39	45.47226775	−2	34	40.9144020	86	0.62	0.37
0237+040		2	39	51.26304399	4	16	21.4119085	160	0.69	0.88
0241+622		2	44	57.69668137	62	28	6.5154803	886	0.65	0.53
0256−005		2	59	28.51615516	0	19	59.9752617	138	0.93	0.37
0300+470	D	3	3	35.24222254	47	16	16.2754406	76	0.81	0.94
0306+102	D	3	9	3.62350016	10	29	16.3409599	99	0.50	0.49
0307+380	D	3	10	49.87992951	38	14	53.8378720	147	0.51	0.31
0309+411	D	3	13	1.96212305	41	20	1.1835585	97	0.50	0.32
0312+100		3	15	21.13979960	10	12	43.0834865	839	0.13	0.13
0316−444		3	17	57.67935755	−44	14	17.1324973	43659	0.10	0.11
0322+222	D	3	25	36.81435154	22	24	0.3655873	91	0.82	0.53
0325+395		3	28	50.31328133	39	40	44.5322072	21262	0.09	0.05
0332−403	D	3	34	13.65451358	−40	8	25.3978415	208	1.88	0.55
0346−279	D	3	48	38.14457723	−27	49	13.5655526	129	0.68	0.60
0402−362	D	4	3	53.74989835	−36	5	1.9131085	73	1.48	1.08
0403−132	D	4	5	34.00338957	−13	8	13.6907083	119	0.69	0.47
0405−385	D	4	6	59.03533560	−38	26	28.0423567	86	1.26	1.43
0410+110		4	13	40.34101427	11	12	14.7860303	519	0.27	0.22
0420−014	D	4	23	15.80072776	−1	20	33.0654034	62	3.78	2.41
0422+004	D	4	24	46.84206092	0	36	6.3293676	96	0.63	0.71
0440−003		4	42	38.66073910	0	17	43.4203921	114	1.25	2.02
0454−463		4	55	50.77252761	−46	15	58.6797411	367	0.74*	
0454−234	D	4	57	3.17922863	−23	24	52.0201418	62	2.17	1.92
0506−612	D	5	6	43.98872791	−61	9	40.9937940	258	1.31*	
0454+844	D	5	8	42.36345199	84	32	4.5440155	503	0.21	0.24

Note: The second column specifies the category of the source in the ICRF2 catalogue (i.e. D for defining source and empty for non-defining). The positions listed here are from the ICRF2 catalogue, and the corresponding uncertainty $\sigma_{pos.}$ is derived from those in α and δ: $\sigma_{pos.} = \sqrt{(\sigma_\alpha \, cos\delta)^2 + \sigma_\delta^2}$. Source names are given in bold face for sources with positional uncertainty larger than 200 µas. The X- and S-band flux density values given here correspond to the mean value of all flux densities measured from VLBI images in the BVID over the years (units in Jy). (*) Those values marked with a star come from Ojha et al. (2004, 2005) and only the X-band value was available.

Table 3: Table 2 (continued).

IERS name		α				δ			$\sigma_{pos.}$ (μas)	X-band flux (Jy)	S-band flux (Jy)
		h	m	s	°	′	″				
0506+101	D	5	9	27.45706864	10	11	44.6000396	100	0.42	0.57
0522−611	D	5	22	34.42547880	−61	7	57.1335242	357	0.47*	
0524+034	D	5	27	32.70544796	3	31	31.5166429	113	0.43	0.42
0528−250		5	30	7.96279681	−25	3	29.8994010	189	0.49	0.91
0529+483	D	5	33	15.86578266	48	22	52.8076620	96	0.68	0.60
0537−441	D	5	38	50.36155219	−44	5	8.9389165	74	3.57	3.82
0536+145	D	5	39	42.36599103	14	33	45.5616993	85	0.53	0.57
0548+378		5	52	17.93691587	37	54	25.2823729	179	0.30	0.32
0552+398	D	5	55	30.80561150	39	48	49.1649664	67	4.50	3.43
0636+680		6	42	4.25740247	67	58	35.6207886	173	0.37	0.42
0642+449	D	6	46	32.02599463	44	51	16.5901237	71	2.73	1.08
0656+082	D	6	59	17.99603428	8	13	30.9533022	74	0.53	0.69
0716+714	D	7	21	53.44846336	71	20	36.3634253	150	1.05	0.57
0722+145	D	7	25	16.80776128	14	25	13.7466902	82	0.59	0.86
0723+219		7	26	14.26073766	21	53	20.1140804	202	0.36	0.31
0736+017	D	7	39	18.03389693	1	37	4.6178588	77	1.23	1.47
0743−006	D	7	45	54.08232111	0	44	17.5398546	113	1.78	1.29
0748+126	D	7	50	52.04573519	12	31	4.8281766	65	2.30	1.23
0804+499	D	8	8	39.66628353	49	50	36.5304035	76	0.86	0.82
0808+019	D	8	11	26.70731189	1	46	52.2202616	63	0.66	0.46
0812+020		8	15	22.96083908	1	54	59.4805839	616	0.24	0.20
0812+367	D	8	15	25.94485739	36	35	15.1488917	99	0.65	0.73
0814+425	D	8	18	15.99960470	42	22	45.4149140	93	0.85	0.88
0821+394		8	24	55.48385101	39	16	41.9040901	92	0.96	0.92
0823+033	D	8	25	50.33835429	3	9	24.5200730	59	1.10	1.09
0823−223		8	26	1.57293454	−22	30	27.2032544	343	0.35*	
0827+243	D	8	30	52.08619070	24	10	59.8204032	76	0.94	0.83
0834+250		8	37	40.24568630	24	54	23.1217065	141	0.44	
0847−120		8	50	9.63562185	−12	13	35.3758201	277	0.59	0.49
0851+202	D	8	54	48.87492702	20	6	30.6408861	60	2.15	1.49
0912+297		9	15	52.40163935	29	33	24.0430020	332	0.11	0.15
0920−397	D	9	22	46.41826064	−39	59	35.0683561	108	1.10	1.09
0925−203	D	9	27	51.82431596	−20	34	51.2324031	103	0.71	0.47
0955+476	D	9	58	19.67163931	47	25	7.8424347	73	1.18	1.12
0954+658	D	9	58	47.24510127	65	33	54.8180587	114	0.84	0.74
1022+194	D	10	24	44.80959508	19	12	20.4156249	82	0.51	0.41
1034−293	D	10	37	16.07973476	−29	34	2.8133345	66	1.39	1.15
1040+244		10	43	9.03576998	24	8	35.4093695	118	0.90	0.68
1039+811	D	10	44	23.06254789	80	54	39.4430277	306	0.57	0.80
1046−409		10	48	38.27117353	−41	14	0.1158878	773	0.23	0.28
1053+815	D	10	58	11.53537962	81	14	32.6751819	279	0.64	0.47
1055+018	D	10	58	29.60520747	1	33	58.8237691	69	3.01	2.50
1101+384	D	11	4	27.31394136	38	12	31.7990644	70	0.35	0.38
1104+728		11	7	41.72259656	72	32	36.0049449	625	0.21	0.15
1111+149	D	11	13	58.69508359	14	42	26.9525965	122	0.28	0.44
1123+264	D	11	25	53.71192285	26	10	19.9786840	77	0.65	1.07
1124−186	D	11	27	4.39244958	−18	57	17.4416582	62	1.45	0.95
1125+366		11	27	58.87081972	36	20	28.3514308	299	0.12	0.17
1143−332		11	46	28.45179042	−33	28	42.6307941	1643	0.21	0.16
1144−379	D	11	47	1.37070177	−38	12	11.0234199	71	1.62	1.28
1145−071	D	11	47	51.55402876	−7	24	41.1410887	69	0.60	0.74
1145+268		11	47	59.76390016	26	35	42.3326801	146	0.41	0.37
1147+245	D	11	50	19.21217405	24	17	53.8353207	90	0.55	0.67

Table 4: Table 2 (continued).

IERS name		α h	m	s	δ °	′	″	$\sigma_{pos.}$ (μas)	X-band flux (Jy)	S-band flux (Jy)
1156+295	D	11	59	31.83390975	29	14	43.8268741	63	1.23	1.18
1212+171		12	15	3.97914173	16	54	37.9570703	177	0.36	0.34
1215+303	D	12	17	52.08196139	30	7	0.6359190	122	0.24	0.27
1219+044	D	12	22	22.54962080	4	13	15.7761797	60	0.73	0.52
1221+809	D	12	23	40.49373854	80	40	4.3404390	322	0.52	0.44
1226+373	D	12	28	47.42367744	37	6	12.0958631	100	0.39	0.36
1236+077	D	12	39	24.58832517	7	30	17.1892686	93	0.71	0.60
1243−072	D	12	46	4.23210358	−7	30	46.5745473	102	0.63	0.73
1244−255	D	12	46	46.80203492	−25	47	49.2887900	81	0.96	0.81
1251−197		12	54	37.25564698	−20	0	56.4087996	1051	0.15	0.17
1252+119	D	12	54	38.25561161	11	41	5.8951798	106	0.43	0.72
1308+554		13	11	3.21082487	55	13	54.3223262	349	0.19	0.23
1313−333	D	13	16	7.98593995	−33	38	59.1725057	81	1.06	0.95
1330+476		13	32	45.24642317	47	22	22.6676990	120	0.32	0.26
1330+022		13	32	53.27053954	2	0	45.6995025	290	0.65	0.33
1333−152		13	36	34.08914571	−15	29	48.0704161	439	0.14	0.17
1333−337		13	36	39.03275288	−33	57	57.0783023	2131	0.18	0.17
1334−127	D	13	37	39.78277768	−12	57	24.6932620	60	4.19	2.48
1342+662	D	13	43	45.95957134	66	2	25.7451011	125	0.39	0.39
1342+663	D	13	44	8.67966687	66	6	11.6438846	141	0.45	0.64
1348+308		13	50	52.73621029	30	34	53.5904749	224	0.24	0.34
1349−439	D	13	52	56.53494294	−44	12	40.3875227	197	0.36*	
1406−076	D	14	8	56.48120036	−7	52	26.6664200	87	0.78	0.66
1424+240		14	27	0.39178893	23	48	0.0376180	327	0.14	0.26
1424−418	D	14	27	56.29756536	−42	6	19.4375991	75	1.83	1.74
1502+106	D	15	4	24.97978142	10	29	39.1986151	67	1.27	1.65
1510−089	D	15	12	50.53292491	−9	5	59.8295878	73	1.90	1.89
1511−100	D	15	13	44.89341390	−10	12	0.2644930	125	0.79	0.77
1514+197	D	15	16	56.79616342	19	32	12.9920178	92	0.60	0.48
1519−273	D	15	22	37.67598872	−27	30	10.7854174	65	1.13	0.95
1538+149		15	40	49.49151734	14	47	45.8848470	82	0.74	0.79
1546+027	D	15	49	29.43684301	2	37	1.1634197	76	1.69	1.34
1548+056	D	15	50	35.26924162	5	27	10.4484262	73	2.42	2.35
1555+001	D	15	57	51.43397128	0	1	50.4137075	79	0.55	0.65
1602−115		16	5	17.53165324	−11	39	26.8307937	242	0.34	0.36
1606+106	D	16	8	46.20318554	10	29	7.7758300	59	1.34	1.65
1636+473		16	37	45.13054817	47	17	33.8311747	142	0.89	0.66
1637+574	D	16	38	13.45629705	57	20	23.9790727	94	1.21	1.13
1705+018	D	17	7	34.41527100	1	48	45.6992837	90	0.55	0.71
1717+178	D	17	19	13.04848160	17	45	6.4373011	90	0.58	0.62
1726+455	D	17	27	27.65080470	45	30	39.7313444	72	0.75	0.82
1730−130	D	17	33	2.70578476	−13	4	49.5481484	72	5.44	4.28
1736+324		17	38	40.50182158	32	24	9.0257504	299	0.10	0.11
1738+499	D	17	39	27.39049252	49	55	3.3684410	117	0.48	0.46
1741−038	D	17	43	58.85613396	−3	50	4.6166450	59	4.31	3.58
1749+096	D	17	51	32.81857318	9	39	0.7284829	59	3.10	1.52
1754+155	D	17	56	53.10213624	15	35	20.8265328	132	0.36	0.28
1758+388	D	18	0	24.76536125	38	48	30.6975330	82	0.85	0.38
1803+784	D	18	0	45.68391641	78	28	4.0184502	211	2.13	2.00
1800+440	D	18	1	32.31482108	44	4	21.9003219	81	0.88	0.65
1759−396		18	2	42.68004643	−39	40	7.9079345	323	1.80	1.44
1823+568	D	18	24	7.06837771	56	51	1.4908371	91	1.14	0.79
1842+681	D	18	42	33.64168915	68	9	25.2277840	139	0.70	0.58

Table 5: Table 2 (continued).

IERS name		\(\alpha \) h	m	s	\(\delta \) °	′	″	$\sigma_{pos.}$ (μas)	X-band flux (Jy)	S-band flux (Jy)
1846+322	D	18	48	22.08858135	32	19	2.6037429	107	0.42	0.49
1849+670	D	18	49	16.07228978	67	5	41.6802978	121	1.08	0.66
1908+484		19	9	46.56276934	48	34	31.8199243	530	0.15	0.16
1908−201	D	19	11	9.65289198	−20	6	55.1089891	65	2.14	2.27
1921−293	D	19	24	51.05595514	−29	14	30.1210524	66	11.21	9.93
1954+513	D	19	55	42.73826837	51	31	48.5461210	97	1.02	0.90
1954−388	D	19	57	59.81927470	−38	45	6.3557585	71	2.33	2.19
1958−179	D	20	0	57.09044485	−17	48	57.6725440	62	1.92	1.37
2008−159	D	20	11	15.71093257	−15	46	40.2536652	86	1.47	0.73
2029+024		20	31	47.25111474	2	39	37.2836171	296	0.34	0.24
2052−474	D	20	56	16.35981874	−47	14	47.6276461	87	1.49	1.42
2059+034	D	21	1	38.83416420	3	41	31.3209577	88	0.69	0.68
2126−158	D	21	29	12.17589777	−15	38	41.0413097	70	1.11	0.87
2127−096		21	30	19.08825689	−9	27	37.4352232	138	0.65	0.46
2131−021	D	21	34	10.30959643	−1	53	17.2387909	91	1.69	1.98
2135−184		21	38	41.92862885	−18	10	44.3753458	19617	0.12	0.18
2136+141	D	21	39	1.30926937	14	23	35.9922096	60	2.04	1.57
2141+175		21	43	35.54457708	17	43	48.7874674	160	0.66	0.43
2142+110		21	45	18.77507729	11	15	27.3123526	246	0.37	0.25
2143−156		21	46	22.97933395	−15	25	43.8856129	102	0.41	0.50
2144+092		21	47	10.16296927	9	29	46.6723567	126	0.76	0.75
2145+082		21	47	55.21940927	8	30	11.8975672	1387	0.19	0.44
2150+173	D	21	52	24.81939953	17	34	37.7950583	84	0.59	0.57
2155−304		21	58	52.06512138	−30	13	32.1181085	176	0.23	0.28
2214+350		22	16	20.00990099	35	18	14.1802625	103	0.43	0.56
2223−052	D	22	25	47.25929302	−4	57	1.3907581	59	4.22	2.90
2227−088	D	22	29	40.08434003	−8	32	54.4353948	85	1.79	1.73
2232−488	D	22	35	13.23657712	−48	35	58.7945006	187	0.82	0.58
2239+096		22	41	49.71729499	9	53	52.4447374	451	0.33	
2254+074	D	22	57	17.30312249	7	43	12.3024770	102	0.36	0.40
2254+024		22	57	17.56309815	2	43	17.5117291	121	0.32	0.16
2255−282	D	22	58	5.96288481	−27	58	21.2567425	66	2.73	1.22
2300−683	D	23	3	43.56462053	−68	7	37.4429706	357	0.64*	
2309+454		23	11	47.40896553	45	43	56.0164564	169	0.40	0.27
2314−409		23	16	46.91998211	−40	41	21.0871784	1188	0.27	0.44
2325+093		23	27	33.58056222	9	40	9.4627727	347	0.78	
2329−384		23	31	59.47613236	−38	11	47.6505007	216	0.46	0.49
2329−415		23	32	19.04840940	−41	18	37.5837399	1258	0.20	0.30
2351−154	D	23	54	30.19518762	−15	13	11.2130207	158	0.56	0.91
2353−686	D	23	56	0.68140587	−68	20	3.4717084	312	0.34*	
2353+816		23	56	22.79391573	81	52	52.2552239	1067	0.45	0.96
2355−106	D	23	58	10.88240761	−10	20	8.6113211	73	0.87	0.80
2357−318	D	23	59	35.49154293	−31	33	43.8242510	296	0.66	0.80